Alkali Metal Modification of the Mo(100) Reconstruction†

Mark L. Hildner*,‡ and Peder J. Estrup

Department of Physics, Brown University, Providence Rhode Island 02912

Received: April 18, 2002; In Final Form: June 11, 2002

LEED studies reveal that the clean Mo(100) surface reconstruction is modified by small amounts of adsorbed K or Na in such a way that the long-range order is maintained but the surface periodicity changes continuously with coverage. The long-range order is also maintained with the adsorption of small amounts of Li, but no periodicity changes are observed. These findings are discussed in relation to driving mechanisms proposed for the clean reconstruction. Although the changes might be attributed to charge-density-wave formation in a qualitative sense, this mechanism appears unable to provide an explanation for the detailed behavior. On the other hand, it appears possible to describe the observed sequence of structures in terms of a local bonding model that includes alkali atom repulsions.

I. Introduction

It is well established that the clean Mo(100) surface undergoes a structural phase transition upon cooling.[1] The discovery of this and the similar W(100) structural transition[1,2] has led to extensive experimental and theoretical studies;[3−12] yet, a determination of the precise driving mechanism remains an unresolved problem in surface science. However, there is little doubt that these reconstructions, involving two isoelectronic bcc transition metals with nearly identical lattice constants, are electronically driven. It would therefore be interesting to have the ability to tune the surface electronic structure and observe the consequent response of these systems. Since alkali metal adsorption may well provide such electronic tuning, we have explored the effects of K, Na, and Li adsorption on the Mo(100) reconstruction.

Discussions about the origin of the reconstructions of the clean (100) surfaces of Mo and W have focused on the relative importance of collective electronic phenomena resulting from two-dimensional (2-D) Fermi surface nesting properties, and of the formation of local bonds. Initial models supposed that the nested sections were sufficiently large to be the sole cause of the reconstruction via the creation of a Peierls type lattice distortion.[3] When photoemission experiments[4] indicated poor nesting, this charge-density-wave (CDW) model was discounted in favor of a Jahn−Teller-like mechanism in which bonding between surface atoms produces a more stable geometry.[5−7] Here, the electrons, unlike in a CDW, are localized in real space so that the surface can lower its energy with many reconstruction wave vectors in contrast to the single nesting wave vector of the CDW. However, subsequent theoretical studies have shown some nonlocal character due to a strong wave vector dependence in the electron−phonon coupling.[6−8] The debate has since been revived by theoretical[8,9] and experimental[10,11] studies which suggest that, after all, Fermi surface nesting contributes significantly to the energy. The additional claim of these studies that the Fermi surface instability is strong enough to be the main cause of the structural change remains a disputed issue and, significantly, a calculation invoking a short-range mechanism not dependent on nesting effects correctly predicts the stability of the experimentally determined low-temperature surface structure.[12]

Although the geometry of clean W(100) has been known for some time, it was not until more recently that structural details of the corresponding Mo surface became available. The signature of the W(100) reconstruction is the (1/2, 1/2) LEED spot due to a two atom $(\sqrt{2} \times \sqrt{2})$R45° unit mesh of p2mg space group symmetry.[1,2] The atomic positions are described by a longitudinal displacement wave with wave vector $\mathbf{q} = 2\pi/a$-(1/2,1/2), and the resulting structure consists of ⟨11⟩ oriented zig-zag chains of W atoms. The LEED pattern for the Mo(100) reconstruction is more complex showing six extra spots in 1/7 order positions along the [11] direction.[13,14] The two closest to the (1/2, 1/2) position are the most intense. The other four have only been observed in more recent diffraction studies and are acutely susceptible to contamination.[14,15] The reconstructed surface has a seven atom $c(7\sqrt{2} \times \sqrt{2})$R45° primitive unit mesh of c2mm space group symmetry. Again, a longitudinal displacement wave describes the atomic positions; however, its harmonic content is dependent on temperature.[14] The fundamental wave vector is $\mathbf{q} = 2\pi/a(3/7,3/7)$, and the structure below 125 K consists of antiphase domains of $[1\bar{1}]$ oriented chains of Mo atoms separated by domain walls comprised of undisplaced atoms;[14,16] this structure can alternatively be viewed as consisting of $3.5\sqrt{2}a$ wide domain stripes in the $[1\bar{1}]$ direction. This structure is illustrated in Figure 1.

Alkali metal adsorption on metal surfaces has been of interest for many years and, in particular, in the past decade because of the discovery of phenomena contradicting the traditional model first proposed by Gurney.[17] This model predicts a partial charge transfer from the adatom to the substrate at low coverage and a subsequent depolarization at higher coverage because of electrostatic interactions between the dipoles. Other predictions of this model are that alkali metals adsorb in high coordination sites and that adatom−adatom interactions are repulsive over a wide coverage range as demonstrated by uniform compression of the overlayer as coverage is increased. These characteristics have been observed in many systems,[18,19] but contrary to the model, several examples of top-site adsorption and a transition

† Part of the special issue "John C. Tully Festschrift".

* To whom correspondence should be addressed. E-mail: hildner@cruzio.com.

‡ Present address: 139 Peach Terrace, Santa Cruz, CA 95060.

10.1021/jp021013x CCC: $22.00
Published on Web 07/20/2002

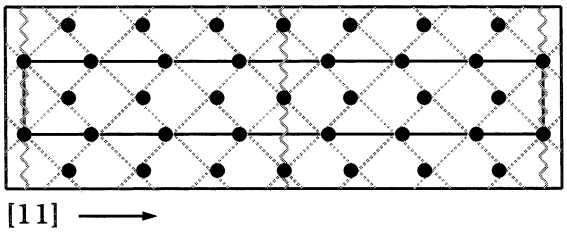

Figure 1. Schematic of the APD structure of the reconstructed Mo(100) surface. The wiggly lines denote the antiphase domain boundaries comprised of undisplaced atoms. The atoms between the domain walls are displaced along the [11] direction to form three [1$\bar{1}$] oriented zig-zag chain structures between each domain wall. Also pictured is the c(7$\sqrt{2}$ × $\sqrt{2}$)R45° unit mesh.

to a condensed phase at low coverage have been recently discovered.[20,21] However, examples of the former have only involved closed packed surfaces where the energy differences of the various adsorption sites can be very small and effects such as substrate rumpling and bond lengths seem to play as significant a role as coordination in determining the lowest energy site.[20] One would therefore expect high coordination sites to be favored on the more open surfaces of Mo(100) and W(100), although the unique electronic characteristics of these surfaces—a half-filled d shell and a strong electron−phonon coupling—may affect the simple picture.[22] It has been pointed out that these same characteristics may also lead to an indirect interaction between adatoms. It is known that an adsorbing species can significantly affect the reconstructions on these surfaces,[23−25] and theoretical studies[26] have shown that a coupling of the substrate distortions induced by individual adatoms can lead to an indirect interaction that can either be attractive or repulsive. This finding has been used to explain experimental observations within the H/W(100), H/Mo(100), and As/Si(100) systems.[24,26]

In this paper, we report the effects of small amounts (coverages ranging from 0.01 to 0.16 ML) of potassium, sodium, and lithium on the Mo(100) reconstruction. These effects are quite surprising for K and Na. In the case of K, we find that adsorption of less than one hundredth of a monolayer is sufficient to cause a change in the position of *all* of the surface Mo atoms. The observed changes suggest a close connection to the driving mechanism of the clean surface reconstruction. We also report evidence of bridge site bonding for K and Na, of center site bonding for Li, of the presence (at higher coverages) of indirect, substrate-mediated adatom−adatom interactions for K and Na, and of the existence of a condensed Li phase that forms below 0.25 ML.

II. Experimental Section

Experiments were performed in an ion-pumped UHV chamber with a typical base pressure below 1×10^{-10} Torr and equipped with a four-grid optics for LEED, a grazing incidence electron gun and a double pass cylindrical mirror analyzer for Auger electron spectroscopy (AES), and a quadrupole mass spectrometer for thermal desorption measurements. The electron gun in the LEED optics was used to make work function measurements by the diode or retarding potential method.

The sample was a single-crystal Mo ribbon of dimensions 2.5 cm × 0.6 cm × 0.25 cm. The sample holder design provided resistive heating and liquid-nitrogen cooling. Sample temperatures ranging from 80 to 2000 K were measured with a W-5%Re/W-26%Re thermocouple spot welded to the back of the sample. Carbon impurities were removed from the sample by repeated cycles of annealing in oxygen at ∼1600 K and flashing in UHV to 2000 K. Cleanliness was determined by AES and by the appearance of an intense, reproducible c(7$\sqrt{2}$ × $\sqrt{2}$)R45° LEED pattern, the latter being the more sensitive monitor.

Potassium, sodium, and lithium atoms were provided by resistively heating SAES Getters alkali metal dispensers positioned ∼2 cm from the sample surface. These sources were thoroughly outgassed and then checked for dose purity (initial by-products were H, CO, and CO_2). The cleanliness of the evaporations was ensured by keeping the pressure rise below 5×10^{-10} Torr and verified by the lack of Mo structural changes of the type known to occur from adsorption of the impurity gases.[27] Accurate and reproducible evaporations were provided by a solid-state timer which could switch the current through the dispenser on and off in desired intervals within a precision of 0.1 s. Relative K coverages were determined by both the peak-to-peak height ratio

$$R_K = \frac{K_{252}(LMM)}{Mo_{186}(MNN)} \quad (1)$$

in AES and by total desorption yield. Relative Na and Li coverages were determined by total desorption yield.

III. Results

The adsorption of K, Na, and Li on the Mo(100) surface was studied up to coverages beyond 1 ML (1 ML corresponds to 1 adatom per Mo surface atom) with LEED, AES, work function, and thermal desorption measurements.[28] The completion of the first layer in each system was signaled by the emergence of a multilayer desorption peak. LEED data for K adsorption at 80 K show a very intense and sharp c(2 × 2) pattern occurring at the completion of the first layer, a nonprimitive (4 × 2) pattern appearing at half that coverage, and a series of intervening overlayer patterns. This sequence leads to the conclusion that the first two patterns occur at K coverages of 0.50 and 0.25 ML and is used to calibrate all absolute K coverages. Similarly, absolute coverages for Na were calibrated with 80 K LEED data which show, from 0.50 to 0.80 ML, a progression of uniformly compressed overlayer patterns, beginning with a sharp c(2 × 2), for which the coverages can be uniquely identified. All of the LEED patterns for these K and Na overlayer structures appear in conjunction with diffraction beams associated with a reconstructed Mo substrate. Both K and Na are most likely in a condensed phase at the completion of the first layer because they have bond lengths of 4.45 and 3.52 Å which are 2% and 4% below that of bulk K and Na, respectively. In the case of Li, the 80 K LEED data show a c(7$\sqrt{2}$ × $\sqrt{2}$)R45° through 80% of the first layer coverage regime after which a (1 × 1) pattern appears. For coverage calibration, it was therefore assumed that the first layer of Li is complete at 1.00 ML. This is reasonable as it implies a Li bond length of 3.15 Å, the Mo lattice constant, which is 4% larger than the bulk Li bond length of 3.02 Å. There is some very interesting physics underlying the phase diagrams of these three systems, but the focus here is on the effects these adsorbates have at low coverage on the substrate structure.

The sequence of LEED patterns observed for small K coverages, θ_K, at 80 K shows a change in the separation or splitting of the extra spots. The clean surface pattern (Figure 2a) contains four extra spots in the (h ± 3/7, k ± 3/7) positions due to two rotationally degenerate domains of c(7$\sqrt{2}$ × $\sqrt{2}$)R45° (the additional beams are observed only when the chamber pressure is low enough). With initial K adsorption,

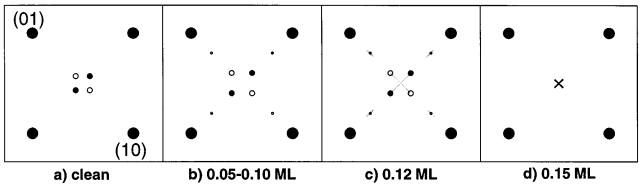

Figure 2. Sequence of LEED patterns for $0 \leq \theta_K \leq 0.15$ ML at 80 K. The extra spots move apart continuously: (a) clean c($7\sqrt{2} \times \sqrt{2}$)R45° due to two domains (filled and open circles); (b) c($5\sqrt{2} \times \sqrt{2}$)R45° with additional spots; (c) inner spots converge and begin to streak; (d) all intensity in streaks.

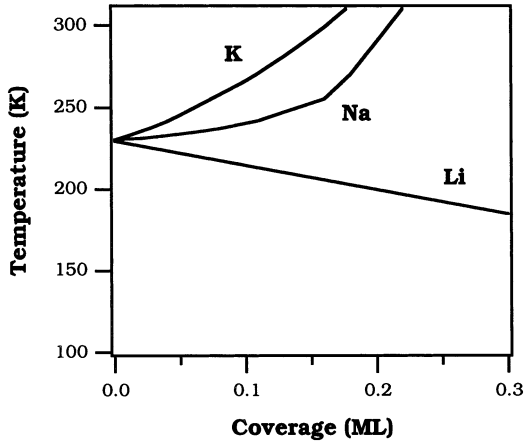

Figure 3. Effect on the transition temperature, T_c, of the Mo(100) reconstruction upon adsorption of K, Na, and Li.

the extra spots move apart and grow in intensity. These spots eventually stop spreading at the (h ± 2/5, k ± 2/5) positions at ~0.05 ML while a new set of spots of lower intensity coincidentally appear and move into the (h±4/5, k±4/5) positions leaving a c($5\sqrt{2} \times \sqrt{2}$)R45° pattern (Figure 2b) which persists until ~0.10 ML. The original spots then converge, begin to streak (Figure 2c), and gradually lose definition with most of their intensity going into the streaks and the new spots disappearing (Figure 2d). Finally, the original spots coalesce and a sharp ($\sqrt{2} \times \sqrt{2}$)R45° pattern is formed (not shown) which remains at all subsequent coverages. In the case of Na adsorption, there is no change in the LEED pattern at very low coverages, but at ~0.04 ML, the spots begin to gradually converge without streaking, and they coalesce at ~0.13 ML. With Li, no changes in the spot splitting are observed as a function of coverage.

The temperature, T_c, at which these Mo structures disorder was also measured. The results are shown in Figure 3. K adsorption increases T_c from the clean surface value by ~95 K at 0.20 ML, and Na adsorption increases T_c by ~60 K near 0.20 ML. In contrast, Li adsorption decreases T_c from the clean surface value by ~30 K at 0.20 ML.

Initial dipole moments for each adsorbate have been calculated from the measurements of the work function change, $\Delta\phi$, using the expression[18]

$$\mu_0 = \frac{1}{2\pi e}\left(\frac{d\Delta\phi}{dn_a}\right)_{n_a \to 0} \qquad (2)$$

where n_a is the density of adsorbate atoms. These values are shown in Table 1.

IV. Discussion

Substrate and Overlayer Structures and Alkali Bonding Site. Plots of the LEED beam splitting versus K and Na coverage are shown in Figures 4 and 5. The splitting, *s*, is defined as the ratio of the distance between the two extra spots and the distance between the (0,0) and (1,1) reflections. The changes in *s* for both adsorbates are continuous as a function of coverage and are observed at hundredths of a monolayer. The extra spots cannot be due to diffraction from overlayers of K or Na because they would require uniform overlayer coverages much higher than those present on the surface—the c($5\sqrt{2} \times \sqrt{2}$)R45° pattern, for example, implies a coverage of 0.20 ML—and they show none of the broadening that would be associated with island formation. There is also no evidence of coexisting phases. Thus, each LEED pattern evolution reflects a continuous change in the Mo substrate structure imposed by a uniform alkali overlayer that is either disordered or lacks enough scattering power to produce a detectable intensity.

TABLE 1: Comparison of the K, Na, and Li Initial Dipole Moments, μ_0, (Expressed in Debye Units) on Mo(100) Calculated from Measured Changes in the Work Function

adatom	μ_0	adatom	μ_0	adatom	μ_0
K	7.1	Na	3.5	Li	1.2

Uniformity of the K and Na overlayers is maintained also at higher coverages (≥0.20 ML) where the aforementioned direct LEED observations become possible. These overlayer structures, in large part, exhibit the uniform compression typical of those seen in other alkali adsorption systems where dipole−dipole interactions predominate.[18,19] The extent to which they do not exhibit this behavior can be explained by the competition of

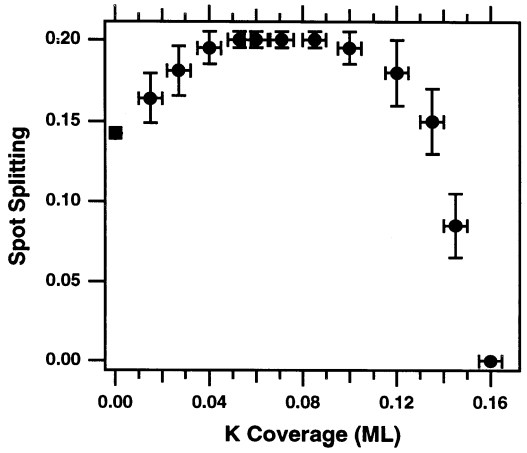

Figure 4. Splitting, *s*, of the extra LEED spots from Mo(100) for the clean surface (square) and as a function of K (circles) coverage.

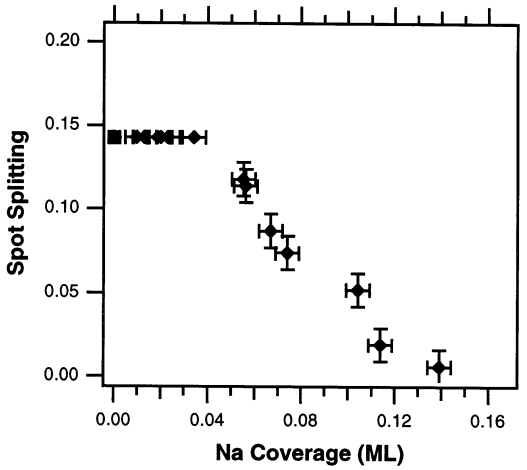

Figure 5. Splitting, *s*, of the extra LEED spots from Mo(100) for the clean surface (square) and as a function of Na (diamonds) coverage.

the dipole−dipole interaction energy with the energetics associated with the adsorbate induced substrate reconstruction[28] as discussed below for the K (4 × 2) structure at 0.25 ML.

All of the low coverage LEED patterns maintain both the 2mm point group symmetry of the clean surface pattern and the symmetry characteristics of a longitudinal distortion mode[29] with wave vector $\mathbf{q} = 2\pi/a[(1 - s)/2,(1 - s)/2]$. The continuous changes in *s* correspond to continuous changes in the average domain size, and the appearance of additional spots, or the streaking of the split spots, reflects changes in the domain width distribution. Initially, the clean surface antiphase domain (APD) structure consists of domains of varying width but with an average wall spacing equal to that of the perfect c($7\sqrt{2} \times \sqrt{2}$)R45° structure so that the LEED pattern shows only the (h ± 3/7, k ± 3/7) spots. With initial adsorption of K, the increase in *s* reveals that the domain walls move closer together, whereas the emergence of the new set of beams shows that the distribution sharpens. This leaves a well ordered c($5\sqrt{2} \times \sqrt{2}$)R45° structure at ∼0.05 ML which is maintained until ∼0.10 ML. Above 0.10 ML, the domain sizes increase, but not smoothly since the split spots streak. The immediate appearance of the streaking implies immediate creation of a very broad distribution implying that walls are being annihilated in addition to moving farther apart. This continues until all domain walls are eliminated leaving a ($\sqrt{2} \times \sqrt{2}$)R45° structure. The fact that this process happens over a very short coverage range—a characteristic seen in Figure 4—is further evidence for wall annihilation. With Na adsorption, the domain wall separation is initially unchanged and then gradually increases until all walls are eliminated.

The observed effects on T_c of the Mo(100) reconstruction are strong indicators of the alkali adsorption sites. It has been shown, within the context of a bonding model of the W(100) reconstruction, that the site of the adsorbate determines the initial slope of the reconstruction phase boundary: T_c is respectively increased, decreased, and unchanged upon adsorption in the bridge, center, and on-top sites[23] which are the three high symmetry sites available for bonding on a bulk terminated W(100) or Mo(100) surface. These predictions have been confirmed experimentally for the H/Mo(100),[24] H/W(100),[25] and O/W(100)[23] systems.

On this basis, the changes in T_c shown in Figure 3 indicate that K and Na, which strengthen the reconstruction, adsorb in bridge sites, whereas Li, which weakens the reconstruction, adsorbs in center sites. Such a conclusion has been substantiated by Kim et al., who have observed similar effects on T_c with K and Li adsorption on W(100).[22] Their density-functional calculations show that the total energy is lowest for Li when it assumes the highest coordination site (4-fold center) on an unreconstructed W surface but lowest for K when it is in a lower coordination site (2-fold bridge) on a reconstructed W surface: the K−W bond energy cost associated with the lower coordination site is less than the energy gain due to dimerization of surface W atoms, which K bridge bonding facilitates.

On the ($\sqrt{2} \times \sqrt{2}$)R45° reconstructed surface and within the domains of the APD structure, the high symmetry sites of the bulk terminated Mo(100) surface have lower symmetry and, in particular, there are two nonequivalent bridge sites, long (LB) and short (SB). These, along with the on-top (T) and center (C) sites, are illustrated in Figure 6. The calculations for the W system[22] show that the alkali binding site is determined by a balance between maximal coordination and reconstruction. Figure 7 illustrates the distortions expected for adsorption in the LB and SB sites when next-nearest neighbor (nnn) top-layer and nearest neighbor (nn) second layer Mo atoms along with nn top-layer Mo atoms are considered. To maximize coordination, the adatom penetrates into the surface; thus, the adatom forces its two nn surface Mo atoms (A and A′ for LB, P and P′ for SB) apart and could draw in the two nnn surface Mo atoms (B and B′ for LB, Q and Q′ for SB) and the second layer Mo atoms. There is a significant difference between the two sites in this model in that occupation of the SB site would reduce the Mo displacements and therefore tend to destabilize the reconstruction. This is in accord with the calculations for the W surface which show K in a long bridge site.[22]

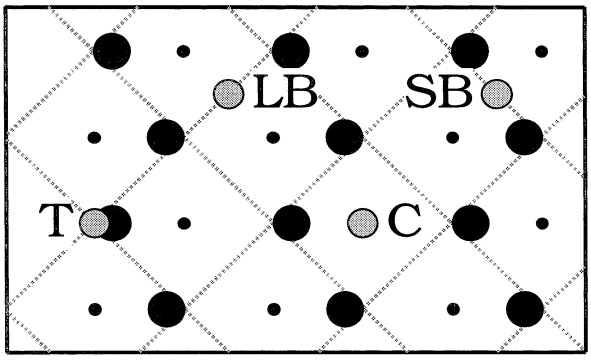

Figure 6. Possible adsorption sites (shaded circles)—(T) on-top, (LB) long-bridge, (C) center, and (SB) short-bridge—within domains of Mo APD structure. Large and small black circles are top and second layer Mo atoms, respectively.

Evidently, the interplay between reconstruction, bonding, and adatom−adatom interaction energies plays a significant role in determining the K and Na overlayer structures observed at coverages ≥0.20 ML. This phenomenon is illustrated with the (4 × 2) structure at $\theta_K = 0.25$ ML. If the structure at this coverage were determined solely by dipole−dipole interactions and registry with the substrate, K would assume a c(4 × 2) structure which is quasihexagonal. Figure 8a shows this structure on the ($\sqrt{2} \times \sqrt{2}$)R45° reconstructed Mo surface with the K atoms in bridge sites. The first or corner atom of the (4 × 2) unit mesh occupies a LB site, whereas the second or center atom assumes a SB site which, as shown above, opposes the reconstruction. Figure 8b shows the four remaining nondegenerate LB sites within the (4 × 2) mesh. We believe that the second K atom assumes site 2 because site 1 gives an unobserved p(2 × 2) structure, the LEED pattern for site 3 would show unobserved extinctions of some of the (4 × 2) beams, and site 4 places K atoms 2.2 Å apart which seems unphysical given the bond-lengths of 4.45 Å for the condensed c(2 × 2) phase and 4.53 Å for bulk K. It is interesting that the second K atom does not assume site 1 and form a p(2 × 2) structure which would also be favored by dipole-dipole repulsions. We conclude that, in assuming site 2, there is an energy gain in the adatom-induced reconstruction which more than compensates for the energy cost associated with adatom repulsions. This can be described as a substrate mediated attractive interaction between adatoms. The progression of overlayer structures at higher coverages for both K and Na exhibits further evidence for such interactions in conjunction with the dipole-dipole repulsions.[28]

Driving Mechanism for Modifications of Mo Reconstruction. Can the evolution of new structures induced by small amounts of K and Na (and the lack thereof with Li adsorption) be explained by either of the two proposed models of the reconstruction driving mechanism? In the CDW mechanism, the changes in **q** are caused by changes in the Fermi surface nesting properties of surface-localized states. The initial changes

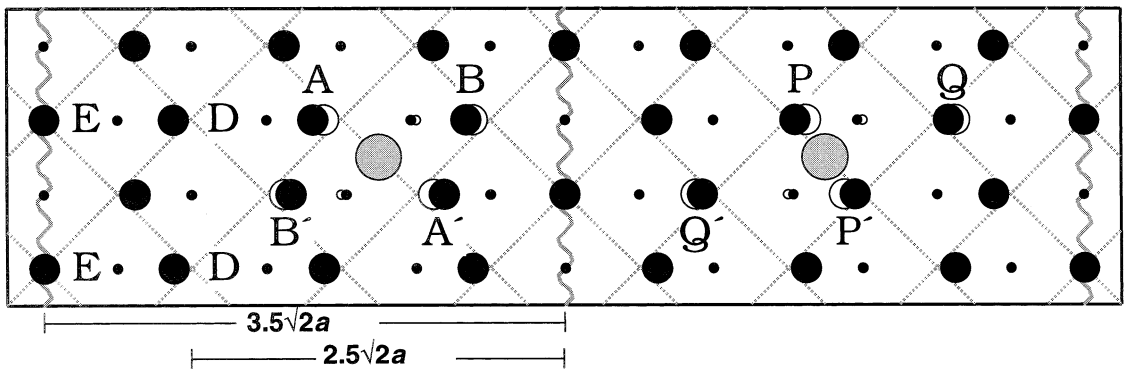

Figure 7. Illustration of local perturbation of both nn (A and A′ for LB, P and P′ for SB) and nnn (B and B′ for LB, Q and Q′ for SB) Mo atoms imposed by adatom. Large shaded circle is adatom; large and small black circles are top and second layer Mo atoms; empty circles are unperturbed Mo positions; and wiggly lines denote antiphase domain boundaries.

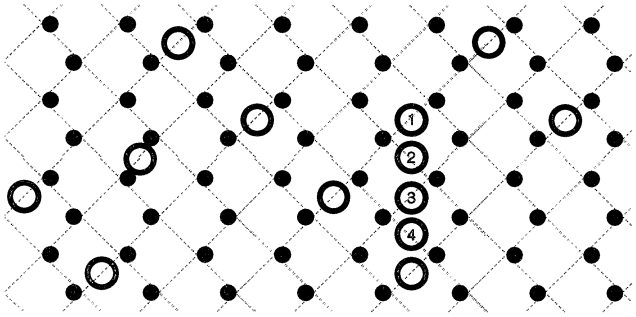

Figure 8. (a) Unobserved c(4 × 2) K structure on the ($\sqrt{2} \times \sqrt{2}$)R45° Mo substrate. Center atom is in a SB site which destabilizes the reconstruction. (b) The four remaining nondegenerate LB sites within the (4 × 2) unit cell.

observed with K adsorption can be explained by a shift in these surface states to energies farther below the Fermi level, E_F, (which is fixed by the bulk metal) as charge is transferred from the electropositive adatoms to the surface.[30,31] Changes in nesting properties would begin immediately and change **q** and *s* according to the dispersion of the nested surface state (SS) band. It should then follow that when Na or Li atoms are adsorbed the same sequence of surface structures should occur, but at slightly different coverages because of the difference in electropositivity. The fact that initially the surface periodicity is unaffected by Na and Li adsorption implies one of these possibilities: (1) that Na and Li have significantly different bonding properties on Mo(100) than K, (2) that the slower change of the crossing wavevector by Na and Li leads to a lock-in to a smaller rational fraction, or (3) that Fermi surface nesting plays little role in determining the Mo structural changes.

However, even if either possibility 1 or 2 is true, it is difficult to explain the increase in **q** (decrease in *s*) that occurs at the end of the K and Na sequences. In the simplest approximation, the changes would be attributed to the nesting properties of a single SS band that is only shifted in energy. In this picture, the reversal of **q** for K implies an unphysical property: either this band bends back on itself or it reverses its energy shift and raises the SS energies to values higher than the clean surface values. Even when changes in the dispersion of the band are invoked, the single nested band picture cannot explain how, with K adsorption, **q** increases much more rapidly than it decreases: the changes in dispersion, like the SS band energy shifts, should change monotonically with the total amount of charge transfer. Although the presence of two SS bands which cross each other above E_F could explain the increase in **q** with K, it could not explain the increase with Na since the crossover point would not be reached with Na adsorption. Furthermore, there is no evidence for such crossing bands in band structure calculations for either the Mo(100) or the W(100) surface.[9,32,33] Thus, although the initial changes may result from CDW, the increase in **q** occurs through some other mechanism. This may be the same mechanism described below within the context of local bonding where, because of steric constraints, adatoms begin to adsorb on sites that lead to the elimination of domain walls.

In a local bonding picture, a new short range structure would be driven by local distortions induced by the adatoms. The long range structure would then depend on the arrangement of the adsorbate overlayer which will be governed in large part by the adatom−adatom interactions. The progression of Mo structures as a function of coverage would be determined by the competition between local adatom-induced substrate distortions and adatom-adatom interactions. Such a model can quantitatively account for all the periodicity changes.

In this model, the adatoms create local distortions and thus change the structural energy of the substrate. Adsorption in some sites raises the structural energy (energy raising or ER site), whereas adsorption in others lowers the structural energy (energy lowering or EL site). The substrate will have a new minimum energy structure with all adatoms in the EL sites. This structure will have a new wavevector and, initially, create a distribution of domain sizes (clean and adsorbate induced) if the local distortions are large enough. However, exclusive occupation of the EL sites imposes restrictions on the overlayer arrangement which leads to a cost in the adatom−adatom (AA) interaction energy. At the lowest coverages, the overlayer is so dilute that adatoms can form overlayer structures that minimize the AA interaction energy without occupying the ER sites. As the coverage increases, exclusive occupation of EL sites increases the AA interaction energy cost. At some critical coverage, θ^c, the AA interaction energy cost with all adatoms in EL sites will exceed the structural energy cost of some adatoms in ER sites. The adatoms will then begin adsorption into ER sites that induce a new, higher energy Mo substrate structure. This higher energy structure may still be a reconstruction, but one with a different wavevector.

We expect that dipole−dipole interactions are significant for K and Na at these low coverages since the LEED data indicate the formation of a uniform (either ordered or disordered) overlayer at these coverages and such interactions are evident from the K and Na overlayer contributions to the LEED patterns at higher coverages. Since the LEED data also show the presence of an attractive substrate-mediated interaction at higher cover-

ages, the possibility that such interactions are significant in the low coverage regime cannot be dismissed. However, with the assumption that dipole−dipole repulsions dominate, the splitting vs coverage progression for both K and Na can be accurately reproduced. If the attractive interactions are then assumed to be significant, the splitting changes occur at different overlayer densities. We therefore conclude, within the context of this model, that the AA interactions for K and Na at these low coverages are dominated by dipole−dipole repulsions.

No assumptions have been made as to what the EL sites are, but all sites (T, C, LB, and SB) within the zig-zag chains of the APD structure are different from those near the domain walls. The EL sites for K and Na must be in the interior of the domains (amongst the zig-zag chains) since, first, the local distortions of surface atoms (which are an integral part of this picture) by K and Na should enhance the reconstruction without initially decreasing the number of domain walls and, second, the structure in these regions is much more like the ($\sqrt{2} \times \sqrt{2}$)R45° Mo surface upon which all K and Na adatoms reside at the end of the progression. The ER sites, on the other hand, are at or near the domain walls of undisplaced Mo atoms because adsorption in these regions will lead to local Mo distortions that will induce a different reconstruction wavevector (one with a lower domain wall density). In summary, the substrate changes periodicity through elimination and annihilation of domain walls resulting from distortions induced by adatoms adsorbing in this region.

This description easily provides a *qualitative* account of all the observed Mo structural changes upon K and Na adsorption. Potassium immediately changes the reconstruction wavevector (and introduces a distribution of clean and adsorbate induced structural domains), and sodium does not because, as seen in the T_c data, K has a stronger influence on the reconstruction. The new locally induced reconstruction wavevector for K is $\mathbf{q} = 2\pi/a(2/5,2/5)$ which differs slightly from that for the clean surface reconstruction, so the LEED pattern shows a splitting reflecting the average domain size and no streaking. Eventually, the K coverage is large enough for the whole Mo surface to be comprised of the K-induced minimum energy structure of c($5\sqrt{2} \times \sqrt{2}$)R45°. With its weaker effect on the reconstruction, Na induces a minimum energy structure that has the same c($7\sqrt{2} \times \sqrt{2}$)R45° periodicity as the clean Mo surface. K and Na adsorb into those binding sites (within the zig-zag chains) that facilitate these structures, but to reduce the AA energy cost, they begin at their respective critical coverages, θ_K^c and θ_{Na}^c, to occupy sites near the domain walls. This locally distorts the Mo surface into a reconstruction having a different, larger wavevector. This critical coverage is smaller for Na even though it has a smaller dipole moment than K: the energy cost of going to another Mo structure is also lower (as evidenced by the weaker effect on T_c) and appears to play the dominant role. Eventually, there is a coverage for each adsorbate where all domain walls have been removed and the ($\sqrt{2} \times \sqrt{2}$)R45° structure remains. Again because of the lower reconstruction energy cost, this coverage is lower for Na. Finally, the Mo surface converges to the ($\sqrt{2} \times \sqrt{2}$)R45° structure less smoothly with K—through wall annihilation in addition to wall shifting as evidenced by streaks in the LEED pattern—for two reasons. First, the domain wall density of the K induced c($5\sqrt{2} \times \sqrt{2}$)R45° is much higher than the Na induced c($7\sqrt{2} \times \sqrt{2}$)R45° (20% instead of 14% of the Mo atoms are undisplaced), and second, the coverage range over which this convergence occurs is smaller for K (~0.7 ML compared to ~0.9 ML).

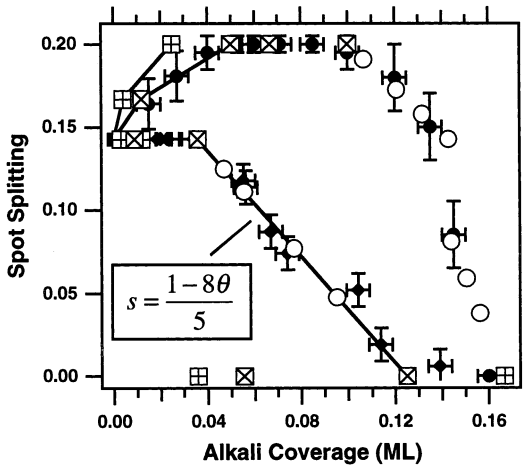

Figure 9. Splitting, *s*, of extra LEED spots from Mo(100) for clean surface (filled square) and as a function of K (filled circles) and Na (diamonds) coverage. The points corresponding to the hexagonal A (squares with ×), hexagonal B (squares with +), and some intermediate (open circles) structures that can be accommodated by the implied substrate periodicities are included. The intermediate points for Na are for the convergence structures shown in Figure 11. There is roughly a linear dependence on coverage within the Na convergence region. Lines connecting the HA and HB points at the lowest K coverages are drawn to aid the eye.

A close examination of the key coverages in this progression reveals a geometrical relationship between the overlayer and substrate. The Mo surface becomes fully c($5\sqrt{2} \times \sqrt{2}$)R45° at $\theta_K \sim 0.05$ ML (one K atom per four Mo unit meshes), begins to converge to ($\sqrt{2} \times \sqrt{2}$)R45° at $\theta_K \sim 0.10$ ML (one K atom per two Mo unit meshes), and arrives at the ($\sqrt{2} \times \sqrt{2}$)R45° at $\theta_K \sim 0.167$ ML (one K atom per three, now smaller, Mo unit meshes). With Na adsorption, the Mo surface begins to converge to ($\sqrt{2} \times \sqrt{2}$)R45° at $\theta_{Na} \sim 0.036$ or 1/28 ML (one Na atom per four Mo unit meshes), and arrives at the ($\sqrt{2} \times \sqrt{2}$)R45° at $\theta_{Na} \sim 0.125$ ML (one K atom per four, now smaller, Mo unit meshes). Furthermore, in the Na convergence region, the splitting vs coverage roughly follows a line connecting these two points. The equation for this line is

$$s = \frac{1 - 8\theta}{5} \tag{3}$$

At specific coverages within this region, the average Mo structure has a rectangular unit mesh of ($n\sqrt{2} \times \sqrt{2}$)R45°, and the corresponding spot splitting is $1/n$ with n increasing from 7. Equation 3 therefore implies a coverage as a function of n given by

$$\theta(n) = \frac{n - 5}{8n} \tag{4}$$

Both sets of splitting vs coverage data are replotted in Figure 9. This line is also included and it matches the experimental results reasonably well. However, the data are insufficiently detailed to determine if the progression is precisely linear. For example, it cannot be ruled out that the surface goes through a series of lock-in transitions and that a staircase trajectory is instead followed.

The local bonding picture imposes these geometrical relationships as can be seen through structural models. Perfect overlayer structures are used in these models, but they are meant only to represent the *average* uniform overlayer structure. Many studies have shown adsorbate structures with nearly uniform interatomic spacing at the lowest detectable (by LEED) coverages[18]—as low

TABLE 2: Parameters for All Type A Quasihexagonal Structures within the Coverage Region of Interest (Lower Coverage Structures Are Excluded for Clarity)[a]

hexagonal A structures: $h = l\sqrt{3}$							
adatom	s	n	l	h	m	θ	allowed
K	0.17	6	12	6.93	7	0.012	yes
			6	3.46	3	0.056	no
	0.20	5	10	5.77	6	0.017	no
			5	2.89	3	0.067	yes
Na	0.14	7	14	8.08	8	0.009	yes
			7	4.04	4	0.036	yes
K & Na	0	1	6	3.46	3	0.067	yes
			4	2.31	2	0.125	yes

[a] All quasihexagonal structures that can be accommodated, without adsorption on domain walls, by the Mo substrate with periodicity $(n\sqrt{2} \times \sqrt{2})$R45° are either of type A or type B (see Table 3). The splitting, s, is $1/n$. The quasihexagonal unit cell is c$(l\sqrt{2} \times m\sqrt{2})$R45° with l dictated by the substrate along [11] and m the closest integer to h. The coverage, θ, is given by $1/(lm)$. Structures that place K atoms in 3.5 $\sqrt{2}$a wide domains or have 2.5 $\sqrt{2}$a wide domains without K atoms are not allowed by the model.

TABLE 3: Parameters for All Type B Structures within the Coverage Region of Interest[a]

hexagonal B structures: $h = l\sqrt{3}$							
adatom	s	n	l	h	m	θ	allowed
K	0.17	6	12	20.78	21	0.004	yes
			6	10.39	10	0.017	no
	0.20	5	10	17.32	17	0.006	no
			5	8.66	9	0.022	yes
Na	0.14	7	14	24.25	24	0.003	yes
			7	12.12	12	0.012	yes
K & Na	0	1	4	6.93	7	0.036	yes
			2	3.46	3	0.167	yes

[a] These have the same meaning as in Table 2.

as 0.07 ML; however, they usually lack long range orientational order. The overlayers in the present study should have a similar uniformity (at least on average) but also orientational order imposed by the avoidance of adsorption near domain walls. This orientational order limits the number of overlayer structures that need to be explored. The most uniformly spaced structures have quasihexagonal arrangements which occur at distinct coverages and can be easily determined. Some structures at intermediate coverages, although more complex, can also be determined with the assumption that adatoms have as uniform a spacing as allowed by the available binding sites.

The quasihexagonal structures have centered rectangular unit meshes with diagonals that make an angle that is close to either 30° (hexagonal A, or HA) or 60° (hexagonal B, or HB) with the [11] direction (perpendicular to the Mo domain walls). The rectangular lattice vectors of these structures have length $l\sqrt{2}$a and $m\sqrt{2}$a in the [11] and [1$\bar{1}$] directions, respectively, where l and m have integral values. The substrate periodicity dictates the value of l, and m is then the value that describes the quasihexagonal structure. To form a true hexagonal structure, l and m would have to satisfy one of the following relationships:

$$m = \begin{cases} \dfrac{l}{\sqrt{3}}, & \text{for HA} \\ \sqrt{3}l, & \text{for HB} \end{cases} \qquad (5)$$

These relationships, of course cannot be satisfied for integral values. Tables 2 and 3 show the nonintegral values of h that do satisfy eq 5 for different values of l for the various K- and Na-induced structures. They then show the closest value of m and the corresponding coverage.

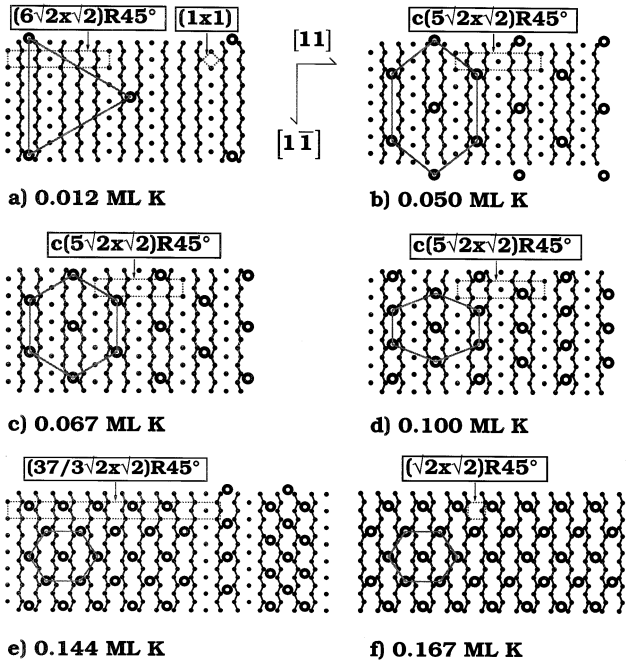

Figure 10. Model structures for K/Mo(100); open circles are adatoms, dots are Mo atoms, and lines connecting Mo atoms show zig-zags. (a)−(d) HA structures; (e) example of intermediate structure; (f) HB structure at point of diffraction beam coalescence. Note the almost perfect hexagonal structure of K in c.

A key aspect of this reconstruction model is that K locally induces the c$(5\sqrt{2} \times \sqrt{2})$R45° structure so the restriction is added that, at low coverages, domain stripes have a width of $2.5\sqrt{2}a$ if they contain K adatoms and of $3.5\sqrt{2}a$ otherwise. This means that some of the K structures in Tables 2 and 3 are not allowed. Also, only even values of l on the $(\sqrt{2} \times \sqrt{2})$R45° structure are considered because odd values would mix bonding sites (either LB with SB or C with T).

This local bonding picture depends not on whether the alkali adsorption site is LB, SB, T, or C but only on the avoidance of wall sites. Figures 10 and 11 show some of the quasihexagonal structures implied by Tables 2 and 3, as well as some intermediate structures, with the adatoms in LB sites. Similar structures with the exact same geometrical relationships can be drawn for each of the other adsorption sites.

Figure 9 includes the allowed points, (s, θ), from Tables 2 and 3 for K quasihexagonal structures. It also includes points for two more HA structures on the c$(5\sqrt{2} \times \sqrt{2})$R45° substrate with $m = 4$ and 2 (the Table 2 value ± 1). At the lowest K coverages, the sequence of HA structures fits the data well; these are presumably chosen over the HB structures as the latter impose, for a given coverage, substrate structures of higher energy. These HA structures and the HB structure at 0.167 ML are shown in Figures 10a−d,f. These structural models strongly support the local bonding model. If the dipole−dipole energetics were comparable to the K-induced reconstruction energetics, the whole surface would not be fully c$(5\sqrt{2} \times \sqrt{2})$R45° until $\theta_K = 0.067$ ML where the overlayer can form the most uniformly spaced overlayer accommodated by the substrate periodicity. Adsorption on walls would also commence shortly thereafter. Instead, the reconstruction energetics are shown to dominate in two ways. First, the whole surface becomes c$(5\sqrt{2} \times \sqrt{2})$R45° at $\theta_K = 0.05$ ML where the next most uniform overlayer structure of lower coverage is formed, and second, adsorption near walls does not begin until $\theta_K = 0.10$ ML where the next most uniform overlayer structure of higher coverage is formed.

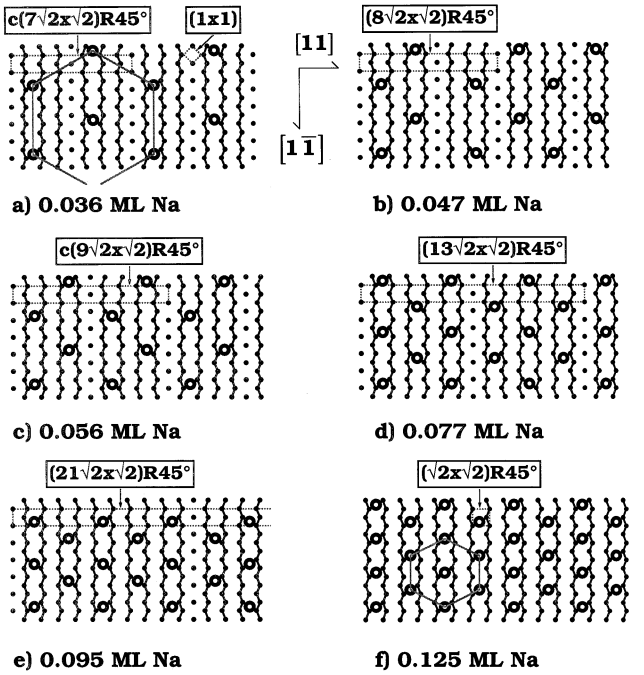

Figure 11. Model structures for Na/Mo(100); symbols are the same as in Figure 10. (a) Nearly perfect hexagonal structure of Na at 0.036 ML after which periodicity begins to change. (b)−(f) Convergence structures; (g) HA structure at point of diffraction beam coalescence.

A possible intermediate structure is shown in Figure 10e; it is a mixture of the 0.10, 0.167, and 0.25 ML structures and also exemplifies the previously described wall annihilation and broad domain size distribution. The points for this and other calculated intermediate structures are included in Figure 9 resulting in a detailed and accurate reproduction of the LEED changes as a function of K coverage.

For Na quasihexagonal structures, Figure 9 includes only the points, (s, θ), from Tables 2 and 3. Here, both the HA and HB structures can be accommodated by the low coverage substrate. Convergence begins after the HA structure at $\theta_{Na} = 0.036$ ML, which is shown in Figure 11a. The local bonding picture is once again validated: this is the highest density Na structure of almost purely uniform spacing that the c($7\sqrt{2} \times \sqrt{2}$)R45° substrate can accommodate, and since Na has a relatively weak effect on the reconstruction, adsorption on walls begins immediately thereafter in order to reduce the dipole-dipole interaction energy.

Figure 11b shows how adsorption on the walls widens every other domain to create a c($8\sqrt{2} \times \sqrt{2}$)R45° structure. The Na adatom arrangement shown is the most uniform for the coverage determined by eq 4. Throughout the convergence region, the Na overlayer continues to compress in both the [11] and [1$\bar{1}$] directions. Once again, the spacing in the [11] direction is dictated by the substrate and gradually reduces from $7\sqrt{2}a$ to $4\sqrt{2}a$. Using eq 4, one can then determine the average spacing in the [11] direction (which gradually reduces from $4\sqrt{2}a$ to $2\sqrt{2}a$) and create the corresponding structural model. Examples of these model structures are shown in Figures 11b−e. The evolution is complete at the HA structure (Figure 11f) at 0.125 ML.

Although this local bonding model can quantitatively account for all of the periodicity changes induced by K and Na regardless of LB, SB, T, or C bonding, LB bonding is in more accord with the model concepts. Adatom induced distortions that enhance the reconstruction are key. It is not intuitive that T and C sites would create such distortions and there is a significant amount of data showing that they do not. In contrast, it is easy to understand how bridge site bonding would create such distortions and there is a significant amount of data that it does. In order for adsorption in SB sites to enhance the reconstruction (to move Mo dimers closer together), the alkali adatom must reside high above the surface. This implies a very low coordination, and there is no evidence for a tendency for alkali adatoms to avoid high coordination at such low coverages in these systems. It is only the LB site that is expected to induce the correct distortions and supplies a high coordination bonding site (as described earlier with Figure 7).

Figure 7 suggests how local distortions from LB bonding may induce the K c($5\sqrt{2} \times \sqrt{2}$)R45° structure. In one local-bond description of the reconstruction mechanism,[12] the incorporation of domain walls lowers the Mo surface energy below that of the simple zig-zag chain structure through reductions in both the average length of the strengthened bonds within the chains and in the average length of the stretched bonds between chains. In this context, a displacement increase for atoms B and B′ would increase, in *opposition* to the walls, the length of the stretched bonds associated with these two Mo atoms. If the resulting tension were significant, it could be relieved by relaxing the displacement of atoms D and moving the domain wall from atoms E to atoms D (and thus increase the domain wall density). The structure in the vicinity of the adatom would then be that of a domain stripe of width $2.5\sqrt{2}a$.

Although it was assumed that dipole−dipole repulsions dominate the AA interactions, an additional interaction is built into the assumptions of this model. In avoiding the ER sites (the domain walls), there is an effective attractive AA interaction. This substrate mediated interaction has some strength at all coverages within this model and is evident in Figures 10e and 11b−e. That such an interaction would be present at these coverages is not unlikely given its appearance at higher coverages.

This local bonding picture is also compatible with the unchanged reconstruction wavevector for Li. It is difficult to determine how Li arranges itself given the lack of any LEED patterns other than the (1 ×1) and c($7\sqrt{2} \times \sqrt{2}$)R45°. Li may be contributing to these patterns, it may be disordered, or it may form other patterns that lack enough scattering power to produce a detectable intensity. However, it is significant that the reconstruction is removed gradually (it is still detectable at 80 K with $\theta_{Li} = 0.80$ ML). We have determined Li binding energies of 43−50 kcal/mol from TDS spectra,[28] and one would expect a uniformly dispersed layer of atoms with binding energies of this magnitude to quickly remove the reconstruction (in contrast, oxygen has similar binding energies and completely removes the reconstruction after 0.2 ML[23]). For example, if it is assumed that Li adsorbs in center sites in either a p(2 × 2) or c(4 × 2) structure (the most uniformly spaced structures at 0.25 ML), all substrate atoms have at least one adjacent adsorption site occupied, and it seems likely that the local distortions would be sufficient to remove the reconstruction at this coverage.

One possible explanation for the slow disappearance of the reconstruction would be the formation of Li coexistence phases of (1 × 1) islands and a dilute gas; at 0.80 ML, roughly 20% of the surface could be reconstructed. Another possibility would be the formation of a single surface phase in which Li has EL and ER sites as proposed previously for K and Na. For Li, which weakens the reconstruction (locally decreases Mo displacements), the EL sites would be within the domain wall region, and the ER sites would be in the interior of the domains, amongst the zig-zag chains. In this case, all initial adsorption

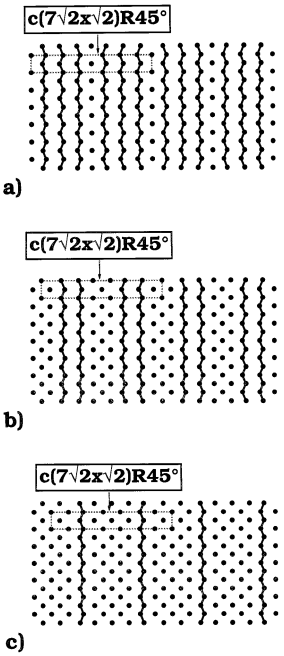

Figure 12. Possible evolution of Mo(100) structures with Li adsorption. In a single c(7$\sqrt{2}$ × $\sqrt{2}$)R45° phase, Li, which removes Mo displacements, would be confined to the domain wall regions. Periodicity of the structure would be maintained by widening of the domain walls.

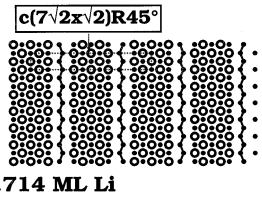

Figure 13. Structure of possible single c(7$\sqrt{2}$ × $\sqrt{2}$)R45° phase with high Li density. Li has ordered domain structure that would produce the same diffraction beams as the substrate.

would be on the domain walls, and as the coverage increases, it would become energetically favorable for adsorption along the zig-zag chains. The substrate periodicity would be preserved by a widening of the domain walls as illustrated in Figure 12. Figure 13 demonstrates how the reconstruction can still be present at high coverages in this scenario. Assuming C site bonding, all sites except those adjacent to the zig-zag chains are occupied, and the corresponding coverage is 0.714 ML. This structure has, at high coverage, (1 × 1) islands of Li, but these islands are highly ordered. In fact, the Li has the same c(7$\sqrt{2}$ × $\sqrt{2}$)R45° unit mesh of the substrate and, if the scattering power is sufficient, would contribute to the diffraction beams of the substrate.

Whether Li forms islands in a coexisting phase or as part of the antiphase domain structure of the substrate ought to be distinguishable in the LEED patterns: coexistence would broaden the integral order beams, particularly at low to medium coverage, and the high coverage antiphase domain structures would produce significant intensity in many of the fractional order beams adjacent to the integral order beams. Neither characteristic was detectable in these experiments. In either case, the implication is that Li begins the formation of a condensed phase at a coverage below 0.25 ML. The driving force for this condensation may either be the formation of attractive, metallic adsorbate bonds or attractive, indirect, substrate-mediated interactions. That one or both of these interactions would dominate at low coverage (in contrast to the dominance of dipole−dipole repulsions for K and Na) is not surprising given the relatively small dipole moment of Li.

V. Conclusion

In summary, we have observed that K, Na, and Li significantly affect the c(7$\sqrt{2}$ × $\sqrt{2}$)R45° Mo(100) reconstruction but in remarkably different ways. Whereas Li decreases the reconstruction transition temperature, T_c, both K and Na increase T_c, with K making the biggest change. Most significantly, K and Na modify the periodicity of the reconstruction, and Li does not. The CDW mechanism offers an appealing physical explanation for the continuous changes in the surface periodicity but appears unable to account for the evolution of structures with increasing wavevector. Although there is a possibility that the initial decrease in wavevector with K adsorption can be explained by CDW, it would be remarkably coincidental that the full c(5$\sqrt{2}$ × $\sqrt{2}$)R45° structure is achieved at a coverage indicative of a simple geometrical relationship between the overlayer and substrate structures. On the other hand, we have shown that a local bonding mechanism can provide a quantitative description of all of the observed periodicities. Here, the surface is unstable to many reconstruction wave vectors, and the structure selected with the addition of K or Na is the one that minimizes the sum of the overlayer electrostatic energy and the substrate energy.

Within this local bonding model, the differing impacts these three alkali metals have on T_c and on the substrate periodicity can be attributed to size differences. Li, being small, assumes center sites because the bond energy cost of assuming the lower coordinated bridge site is too great, and the structure becomes dominated by attractive AA interactions at low coverage because Li has a small dipole moment. The results are a destabilization of the reconstruction (a lowering of T_c) without a change in the substrate periodicity where the reconstruction persists. K and Na assume bridge sites because they are large enough for the energy gain of a reconstructed Mo substrate to outweigh the bond energy costs. This stabilizes the reconstruction (raises T_c) and, at high enough coverage, changes the substrate periodicity when adatoms must—because of significant dipole−dipole repulsions—adsorb on and eliminate domain walls. K, being larger than Na, imposes a larger perturbation on the substrate which consequently leads to a greater stabilization of the reconstruction, to immediate changes in the periodicity, and to more resistance (despite K having a larger dipole moment) to the removal of the domain walls.

Of course, the particular model that we have proposed does depend on some characteristics of alkali metal adsorption on this surface determined by indirect evidence. These characteristics need to be confirmed in further investigations of these systems.

Note Added after ASAP Posting. This article was released ASAP on 7/20/2002 with minor errors in Tables 2 and 3. The correct version was posted on 7/25/2002.

Acknowledgment. This work was supported by the National Science Foundation

References and Notes

(1) Felter, T. E.; Barker, R. A.; Estrup, P. J. *Phys. Rev. Lett.* **1977**, *38*, 1138.

(2) Debe, M. K.; King, D. A. *J. Phys. C* **1977**, *10*, L303.

(3) See, e.g.: (a) Tosatti, E. *Solid State Commun.* **1978**, *25*, 637. (b) Krakauer, H.; Posternak, M.; Freeman, A. J. *Phys. Rev. Lett.* **1979**, *43*, 1885.

(4) Campuzano, J. C.; Inglesfield, J. E.; King, D. A.; Somerton, C. *J. Phys. C* **1981**, *14*, 3099.
(5) Inglesfield, J. E. *J. Phys. C* **1979**, *12*, 149.
(6) Terakura, I.; Terakura, K.; Hamada, N. *Surf. Sci.* **1981**, *103*, 103.
(7) Tomásek, M.; Pick, S. *Surf. Sci.* **1984**, *140*, L279.
(8) Wang, X. W.; Chan, C. T.; Ho, K. M.; Weber, W. *Phys. Rev. Lett.* **1988**, *60*, 2066.
(9) Haas, H.; Wang, C. Z.; Ho, K. M.; Fähnle, M.; Elsässer, C. *Surf. Sci.* **2000**, *457*, L397.
(10) Chung, J. W.; Shin, K. S.; Baek, D. H.; Kim, C. Y.; Kim, H. W.; Lee, S. K.; Park, C. Y.; Hong, S. C.; Kinoshita, T.; Watanabe, M.; Kakizaki, A.; Ishii, T. *Phys. Rev. Lett.* **1992**, *69*, 2228.
(11) Smith, K. E.; Kevan, S. D. *Phys. Rev. B* **1991**, *43*, 3986.
(12) Roelofs, L. D.; Foiles, S. M. *Phys. Rev. B* **1993**, *48*, 11287.
(13) Hildner, M. L.; Daley, R. S.; Felter, T. E.; Estrup, P. J. *J. Vac. Sci. Technol. A* **1991**, *9*, 1604.
(14) Daley, R. S.; Felter, T. E.; Hildner, M. L.; Estrup, P. J. *Phys. Rev. Lett.* **1993**, *70*, 1295.
(15) Smilgies, D.-M.; Hulpke, E. *Phys. Rev. B* **1991**, *43*, 1260.
(16) Smilgies, D.-M.; Eng, P. J.; Robinson, I. K. *Phys. Rev. Lett.* **1993**, *70*, 1291.
(17) Gurney, R. W. *Phys. Rev.* **1935**, *47*, 479.
(18) Aruga, T.; Murata, Y. *Prog. Surf. Sci.* **1989**, *31*, 61.
(19) Diehl, R. D.; McGrath, R. *Surf. Sci. Rep.* **1996**, *23*, 43.
(20) Diehl, R. D.; McGrath, R. *J. Phys.: Condens. Matter* **1997**, *9*, 951.
(21) Neugebauer, J.; Scheffler, M. *Phys. Rev. Lett.* **1993**, *71*, 577.
(22) Kim, H. W.; Ahn, J. R.; Chung, J. W.; Yu, B. D.; Scheffler, M. *Surf. Sci.* **1999**, *430*, L515.
(23) Roelofs, L. D.; Chung, J. W.; Ying, S. C.; Estrup, P. J. *Phys. Rev. B* **1986**, *33*, 6537.
(24) Prybyla, J.; Estrup, P. J.; Chabal, Y. J. *J. Chem. Phys.* **1991**, *94*, 6274.
(25) Barker, R. A.; Estrup, P. J. *J. Chem. Phys.* **1981**, *74*, 1442.
(26) Tiersten, S. C.; Reinecke, T. L.; Ying, S. C. *Phys. Rev. B* **1989**, *39*, 12575.
(27) Semancik, S.; Estrup, P. J. *J. Vac. Sci. Technol.* **1980**, *18*, 541.
(28) Hildner, M. L. Ph.D. Thesis, Brown University, Providence, RI, 1992.
(29) Barker, R. A.; Semancik, S.; Estrup, P. J. *Surf. Sci.* **1980**, *94*, L162.
(30) Wimmer, E.; Freeman, A. J.; Hiskes, J. R.; Karo, A. M. *Phys. Rev. B* **1983**, *28*, 3074.
(31) Soukiassian, P.; Riwan, R.; Lecante, J.; Wimmer, E.; Chubb, S. R.; Freeman, A. J. *Phys. Rev. B* **1985**, *31*, 4911.
(32) Ohnishi, S.; Freeman, A. J.; Wimmer, E. *Phys. Rev. B* **1984**, *29*, 5267.
(33) Mattheiss, L. F.; Hamann, D. R. *Phys. Rev. B* **1984**, *29*, 5372.